Journal of Engineering Mathematics (2006) 55: 127–150
DOI 10.1007/s10665-005-0191-8

Regular wave impact onto an elastic plate

A.A. KOROBKIN* and T.I. KHABAKHPASHEVA
*Lavrentyev Institute of Hydrodynamics, Novosibirsk 630090, Russia (*Author for correspondence; E-mail: kaa@hydro.nsc.ru)*

Received 12 March 2004; accepted in revised form 4 January 2005 / Published online: 14 July 2006

Abstract. A computational analysis of an elastic plate dropped against regular long waves is presented. The problem is considered within the linear potential-flow theory. The liquid flow is two-dimensional and the plate is modelled by an Euler beam. The analysis is based on the normal-mode method with hydroelastic behavior of the plate being of main interest. Different impact conditions are considered to study the dependence of the total energy of the plate–liquid system on impact geometry and plate properties. The contributions of kinetic and potential energies to the total energy are analyzed. It is shown that the kinetic part of the system energy is small at the instant of time when bending stresses in the beam approach their maximum values. Estimations of both the total energy and the maximum of bending stresses are presented. Most of the calculations are performed for the conditions of experiments carried out in MARINTEK. A range of the problem parameters is also considered, to reveal peculiarities of the unsteady interaction between a falling elastic plate and surface waves.

Key words: energy-conservation law, hydroelasticity, maximal bending stresses, normal-mode method, water impact

1. Introduction

The plane unsteady problem of an elastic plate falling down onto a liquid free surface covered with regular long waves is considered. Initially ($t'=0$), the plate touches the wave profile and starts moving downwards thereafter with a constant velocity V (see Figure 1). The position of the left edge of the plate at the initial moment is taken as the origin of the Cartesian coordinate system $x'Oy'$ (dimensional variables are denoted by a prime). The waves are assumed linear. The wave shape before impact is described by the equation

$$y' = a[\cos(\nu[x' - x'_1] - \omega t') - 1], \tag{1}$$

where a is the wave amplitude, ω is the wave frequency, ν is the wavenumber, $\omega^2 = g\nu$ for deep water, x'_1 is the distance of the impact point from the left edge of the plate, g is the gravity acceleration, and $T_W = 2\pi/\omega$ is the wave period. The wave is assumed long, that is $a\nu \ll 1$. The plate length $2L$ and the wave length $\lambda = 2\pi/\nu$ are of the same order, hence we have also $a/L \ll 1$. The impact velocity is assumed to be much less than the sound velocity in a liquid at rest, c_0. Initially the plate is horizontal and undeformed. It corresponds to the interval $y'=0,\ 0<x'<2L$.

The shape of the plate is changed owing to its interaction with the liquid. The plate is dry at the initial moment, $t'=0$, and only partially wetted in the first stage of the process, which is referred to as the impact stage. During the second stage (penetration stage), the plate is totally wetted and continues to interact with the liquid. The presence of the contact points between the free surface and the elastic plate during the impact stage is the main feature of the problem. The positions of these points are unknown in advance and must be determined together with the liquid flow and the plate deflections. We shall determine the plate deflection

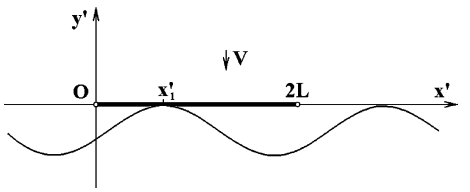

Figure 1. Elastic plate and the free surface at the time of impact.

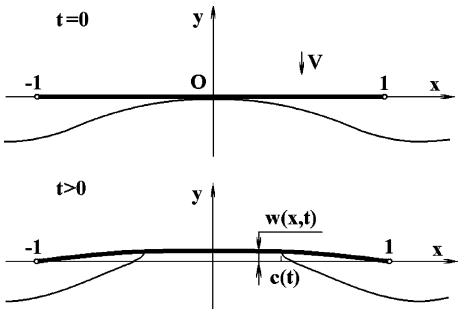

Figure 2. Central impact.

and bending stresses in the plate, estimate the maximum stresses and analyze their dependence on impact conditions, initial shape of the liquid free surface and properties of the plate.

The analysis is based on the following assumptions: (A1) the liquid is ideal and incompressible; (A2) the liquid flow is two-dimensional and potential; (A3) the plate deflection is governed by the Euler beam equation; (A4) the beam edges are simply supported; (A5) the influence of the air, as well as both external mass forces and surface tension, are negligibly small; (A6) the wave length is comparable to the beam length; (A7) the wave amplitude is much smaller than the beam length; (A8) the duration of the impact stage T_i is much smaller than the greatest period of free vibrations of the plate on the liquid surface T_1 and much greater than the time scale L/c_0 of the acoustic effects; (A9) the elastic plate is the bottom of a rigid structure which penetrates the liquid with a constant velocity V; (A10) during the impact stage the contact points move monotonically with time; (A11) the ratio VT_1/L is much less than unity.

Motivations for the present research come from ship hydrodynamics, where wave impact onto the wetdeck of a catamaran can be very severe and may lead to local damage of the wetdeck. This problem has been intensively studied experimentally during the last ten years [1,2], numerically [2–6] and theoretically [2,7]. The study carried out by Norwegian researchers is based exclusively on the experiments by Aarsners [1]. Attempts to generalize the derived predictions to other experiments (see, for example, [8,9]) were not done (see [2]). It should be noted that other experiments have not been subjected to such intensive theoretical analysis as the Norwegian ones. A preliminary theoretical analysis of the experiments by Zhu and Faulkner [9] was given by Korobkin [10] with three-dimensional effects taken into account. The present study is based only on the Norwegian experiments. In addition to the theoretical analysis already carried out by Faltinsen and his group: we

(1) use a modified method of normal modes. After the proposed modifications: calculations of the hydrodynamic loads are not required; the matrix of hydrodynamics coefficients is evaluated analytically; the positions of the contact points are governed by ordinary differential equations, which are incorporated into the system for the principal coordinates of the normal modes; there are no obstacles to start numerical simulations from the initial moment, at which the size of the wetted area is zero; there is no need to introduce the acoustic stage to describe formation of the contact region from a single point;
(2) focus on global characteristics of the interaction, which make it possible to explain energy redistribution during the impact and to estimate maximum stress amplitude;
(3) consider a range of the problem parameters to reveal peculiarities of the interaction. This may be helpful to design future experiments on elastic-plate impact.

It is worth noting that assumptions (A8) and (A11) in this paper provide some limitations. The greatest period of free vibrations of the plate placed in an unbounded liquid, T_1, is of the order $O([\rho L^5/EJ]^{1/2})$, where ρ is the liquid density, E is the elasticity modulus, J is the inertia momentum of the beam cross-section, $J = h^3/12$ for a beam of constant thickness h [2]. For a plate of length $2L$, which is comparable with the wavelength λ, the duration of the impact stage T_i is of the order $O(a/V)$. In order to consider also the case of very long regular waves with $2L \ll \lambda$, the radius of the curvature at the wave crest, R, is introduced, where $R = (a\nu^2)^{-1}$. The wave profile can be approximated by the parabolic contour $y' = -(x' - x_1')^2/(2R)$ close to the impact point. Neglecting both the free-surface deformation and the plate deflection during the impact stage, we can estimate the order of the impact stage duration as $L^2/(RV)$. This quantity is of the same order as a/V, where $L/\lambda = O(1)$, and of higher order, where $L/\lambda \ll 1$. Assumption (A8) provides the inequalities

$$\frac{L}{c_0} \ll \frac{L^2}{RV} \ll \sqrt{\frac{\rho L^5}{EJ}},$$

which lead to the following limitations for the impact velocity

$$[EJ/\rho L]^{1/2} \ll VR \ll c_0 L. \tag{2}$$

Experiments [5] were performed under the following conditions: $L = 0{\cdot}25$ m, $E = 21 \times 10^{10}$N/m^2, $\rho = 10^3$ kg/m^3, $h = 0{\cdot}008$ m, $c_0 = 1500$ m/s. We obtain $(EJ/\rho L)^{1/2} \approx 6$ m^2/s and $c_0 L \approx 375$ m^2/s. If the product VR approaches the lower bound in (2), the quantities T_i and T_1 are comparable to each other. If the product approaches the upper bound, $c_0 L$, acoustic effects must be taken into account during the impact stage [11]. Assumption (A8) is essential for theoretical analysis because it makes possible to separate the impact stage, during which large impact forces occur, and the penetration stage, at which the bending stresses approach their maximum values, and also to disregard the acoustic stage of the impact [2].

Assumption (A11) gives $V \ll 24$ m/s. This inequality guarantees that the bending stresses take their maximum values sufficiently before the penetration depth of the plate becomes comparable to the length scale L of the problem. Assumptions (A7) and (A11) indicate that, as a first approximation, we can put the boundary conditions on the line $y' = 0$ and to linearize them and the equations of motion. The ratio L/R, which is small, can be taken as the parameter of linearization.

At the leading order the liquid flow before the impact can be neglected compared to the flow caused by the impact for $t'/T_1 = O(1)$ if and only if $T_w \gg T_1$. We obtain $T_1 \approx 0{\cdot}01$ s, which is much smaller than the period 0·7–5·0 s of regular waves used in the experiments [2]. Therefore, within the experimental conditions, wave motion can be neglected and the liquid can be considered as being at rest at the impact instant with its free surface described by Equation (1), where $t' = 0$.

It should be noted that, even after all possible simplifications, the problem is coupled (hydrodynamic loads are dependent on the beam deflection and vice versa) and nonlinear at the impact stage (the dimension of the contact region is unknown in advance and has to be determined together with the liquid flow and the beam deflection). At the penetration stage the problem is linear and its solution can be readily found if the beam deflection and velocities of beam elements are given at the beginning of this stage. Those values are determined by the nonlinear solution of the problem at the impact stage.

Both the impact stage and the penetration stage of the plate–liquid interaction are analysed for the three main cases: (i) central impact (Figure 2); (ii) edge impact (Figure 3); (iii)

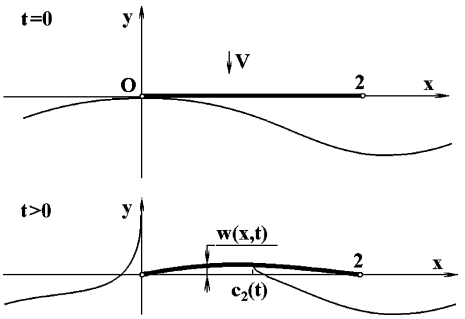

Figure 3. Edge impact.

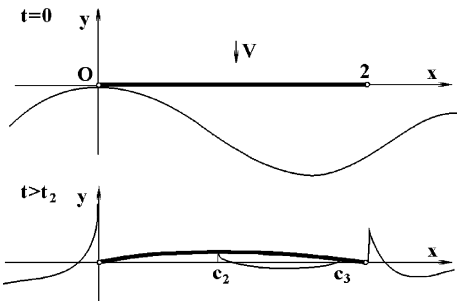

Figure 4. Impact with attached cavity.

impact with a cavity formation (Figure 4), with the help of the normal-mode method [3]. After the modifications [12] this method leads to an infinite system of ordinary differential equations with respect to the principal coordinates of the beam deflection and dimensions of the contact region. Computer programs developed for the three distinguished cases are combined to describe plate impact under arbitrary impact conditions.

Numerical simulations are performed to determine details of the plate/liquid interaction during both the impact stage and the penetration stage, the kinetic energy of the plate, its potential energy and the kinetic energy of the liquid flow. It was found that, in spite of the short duration of the impact stage, the peculiarities of the initial shape of the free surface and the impact conditions are of great importance, the hydrodynamic loads are very high and are dependent on the velocity of the contact-region expansion [13]. In the case of edge impact it was revealed that, within the framework of the incompressible liquid model, the velocity of the contact-region expansion and, therefore, the hydrodynamic loads on the beam, can be beyond all bounds owing to the flexibility of the beam. This phenomenon is of a geometrical nature and occurs when the angle between the beam and the liquid free surface close to the periphery of the contact region tends to zero. In naval hydrodynamics this phenomenon is known as bow-flare slamming. In the case of impact with cavity formation, the loads are unbounded for any parameters of the beam and waves. This is due to the fact that the angle between the free surface and the plate at the contact points is very small at the moment the cavity collapses. In this case the contact region consists of two parts which are separated by a cavity. In this study the presence of air in the cavity is not taken into account.

The mathematical formulation of the problem and a general description of the present approach are given in Section 2. Modifications of the normal-mode method are presented in Section 3 for the simplest case of central impact. In Section 4 the method is applied to the problem of edge impact, which is a part of the original problem. Peculiarities of the impact stage are discussed and comparisons of the beam behaviors at the end of the impact stage for both central impact and edge impact are presented. Elastic-plate impact with a cavity formation is analyzed in Section 5. Vibration of the plate during the penetration stage is studied in Section 6 with a focus on a comparison between the theoretical predictions and the experimental results. One of the features of the theoretical prediction for maximum bending-stress evolution is the overestimation of higher-mode contributions. Generation of high-frequency components of the bending stresses is investigated in Section 7. Global characteristics of the plate impact and their evolutions in time are studied in Section 8. The energy-conservation law and the results of numerical simulations of the impact are used in Section 9 to derive estimates of maximum bending-stress amplitude. The main results of the present study are outlined in Section 10.

2. Formulation of the problem

The plane problem of elastic-beam impact onto the slightly curved free surface of an ideal incompressible liquid is considered in non-dimensional variables. The scales of the independent variables are chosen the same as in the rigid-body impact problem. They are: L is the length scale, $L^2/(RV)$ is the time scale, V is the velocity scale, $\rho V^2 R/L$ is the pressure scale, Eh/R is the bending-stress scale. In numerical analysis we use scales that characterize the impact stage. Generally speaking, we need to introduce other scales [2] to describe the process during the penetration stage. In particular, it is reasonable to take T_1 as the time scale of the penetration stage and the product VT_1 as the displacement scale. However, the description of the penetration stage is much simpler than that of the impact stage. That is why we do not expect any difficulties with its numerical study, even if the choice of scales for the penetration stage are not optimal. More details about the orders of the unknown quantities during the penetration stage can be found in [2] and [14].

Within the framework of the linearized impact theory, which is referred to as the Wagner theory [15], the flow domain coincides with the lower half-plane $y<0$. The liquid flow is governed by the Laplace equation for the velocity potential $\varphi(x, y, t)$, and the plate deformation by the Euler beam equation for the plate deflection $w(x, t)$. The conditions on the liquid boundary are linearized and imposed on the line $y=0$. A part of the boundary $x \in D(t),\ y=0$ corresponds to the contact region of the elastic beam with the liquid, and the part $x \notin D(t)$, $y=0$ corresponds to the free surface where the pressure is zero at all times. Despite the fact that both the equations of motion and the boundary conditions are linearized, the problem is still nonlinear because the contact region $D(t)$ is unknown in advance. The coupled problem has the form

$$\alpha \frac{\partial^2 w}{\partial t^2} + \beta \frac{\partial^4 w}{\partial x^4} = p(x, 0, t) \ (0<x<2,\ t>0), \tag{3}$$

$$w = w_{xx} = 0 \ (x=0,\ x=2,\ t \geq 0), \tag{4}$$

$$w = w_t = 0 \ (0 < x < 2,\ t=0), \tag{5}$$

$$p = -\varphi_t \qquad (y \leq 0), \tag{6}$$

$$\varphi_{xx} + \varphi_{yy} = 0 \qquad (y < 0), \tag{7}$$

$$\varphi = 0 \ (y=0,\ x \notin D), \tag{8}$$

$$\varphi_y = -1 + w_t(x, t) \ (y=0,\ x \in D), \tag{9}$$

$$\varphi \to 0 \qquad (x^2 + y^2 \to \infty). \tag{10}$$

Here $p(x, y, t)$ is the hydrodynamic pressure, $D(t) \subset [0, 2], \alpha = M_B/(\rho L),\ \beta = EJ/(\rho L R^2 V^2)$, M_B is the beam mass per unit length. In dimensionless variables the bending-stress distribution on the upper side of the beam $\sigma(x, t)$ is given as $\sigma(x, t) = w_{xx}(x, t)/2$. In non-dimensional variables the shape of the plate with respect to the initial position of the liquid free surface is described by the equation $y = (L/R) y_b(x, t)$,

$$y_b(x, t) = \frac{1 - \cos[\eta(x - x_1)]}{\eta^2} - t + w(x, t), \tag{11}$$

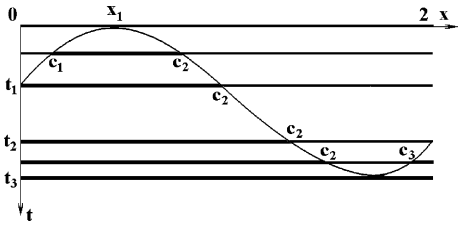

Figure 5. Three phases of the impact stage.

where $\eta = 2\pi(L/\lambda)$ and L/R is the parameter of linearization. In particular, for very long waves, $\eta \to 0$, and close to the impact region, $|x - x_1| = O(1)$, Equation (11) leads to the parabolic approximation of the wave profile

$$y_b(x,t) \approx \frac{1}{2}(x - x_1)^2 - t + w(x,t).$$

This approximation was used in [12] and [16].

Initially ($t = 0$), the beam touches the liquid free surface at a single point x_1, where $0 \le x_1 \le 1$ (Figure 5). Central impact corresponds to $x_1 = 1$, and edge impact to $x_1 = 0$. In the general case ($0 < x_1 < 1$) the dimension of the contact region, which appears at the impact moment, is described by two functions $c_1(t)$ and $c_2(t)$, where $\mathrm{d}c_1/\mathrm{d}t < 0$ and $\mathrm{d}c_2/\mathrm{d}t > 0$ according to assumption (A10) and $c_1(0) = c_2(0) = x_1$. During the first part, $0 < t < t_1$, of the impact stage we obtain $D(t) = \{x \mid c_1(t) < x < c_2(t)\}$, where $c_1(t_1) = 0$. During the second part, $t_1 < t < t_2$, the dimension of the contact region is described by the function $c_2(t)$ and $D(t) = \{x \mid 0 < x < c_2(t)\}$. It should be noted that, for simplicity, both the deformations of the liquid free surface and the beam deflection are not shown in Figure 5. Wetted parts of the plate are shown with thick lines and the dry parts with thin lines.

It is possible that the right edge of the beam touches the disturbed liquid free surface well before the plate is totally wetted. If so, a cavity is formed close to this edge. The cavity collapses thereafter if no air is entrapped. Two reasons may be responsible for this scenario. They are: (1) special shape of the initial free surface (see Figure 4); (2) elastic deflection of the beam (blockage phenomenon). In any case, the second part of the contact region may appear, the dimension of which is described by the function $c_3(t)$ (Figure 5). In this case $D(t) = \{x \mid 0 < x < c_2(t),\ c_3(t) < x < 2\}$. This part of the impact stage, $t_2 < t < t_3$, is referred to as the third phase. This phase is over at the instant t_3, when the cavity collapses, $c_2(t_3) = c_3(t_3)$.

The penetration stage starts at $t = t_3$. During this stage the problem is linear but coupled. It should be noted that, for given impact conditions, some phases may be absent. For example, in the central-impact problem studied in Section 3, there is only the first phase with $c_1(t) = 2 - c_2(t)$.

The initial conditions for the first phase are given by (5) and for both the following phases and for the penetration stage it is required that the beam deflection $w(x,t)$ and its first derivative in time $w_t(x,t)$ change continuously at $t = t_j$, $j = 1, 2, 3$,

$$w(x, t_j + 0) = w(x, t_j - 0), \qquad w_t(x, t_j + 0) = w_t(x, t_j - 0). \tag{12}$$

The formulation of the problem will be completed once equations for the functions $c_1(t), c_2(t)$ and $c_3(t)$ have been obtained. Those equations follow from the condition that the displacements of the liquid particles are finite at the contact points: $x = c_1(t)$ and $x = c_2(t)$ for $0 < t < t_1$, at $x = c_2(t)$ for $t_1 < t < t_2$, and at $x = c_2(t)$ and $x = c_3(t)$ for $t_2 < t < t_3$. The equations

are derived for each phase separately. They are equivalent to the well-known Wagner conditions [13]. Wagner conditions in their traditional forms lead to systems of singular, nonlinear integral equations [2], which are not easy to solve numerically, even for undeformable bodies. This is why modified Wagner conditions are used here [13]. Modified Wagner conditions are transformed to nonlinear ordinary differential equations, which are incorporated into the system for principal coordinates of the beam deflection.

3. Central impact

The problem, where initially the wave crest touches the plate centre, is the simplest one. In this case it is convenient to take the middle point of the plate as the origin of the Cartesian coordinate system xOy (in this section only). The initial shape of the free surface is symmetrical with respect to the Oy-axis, which indicates that the flow is also symmetrical with respect to the new coordinate system (Figure 2). The central-impact problem has the same features as the problem for the first part of the impact stage but it is more suitable to demonstrate the main peculiarities of both the method of analysis and the numerical algorithm.

The contact-region dimension is described by a function $c(t)$, where the interval $y=0$, $-c(t)<x<c(t)$ corresponds to the wetted part of the plate. In the new coordinate system Equation (11) is replaced by

$$y_b(x,t)=\eta^{-2}(1-\cos(\eta x))-t+w(x,t), \tag{13}$$

where $w(-x,t)=w(x,t)$. For the symmetrical case the Wagner condition leads to the equation [13]

$$\int_0^{\pi/2} y_b[c(t)\sin\theta,t]\,\mathrm{d}\theta=0. \tag{14}$$

Substitution of (13) in (14) gives

$$t=\frac{1-J_0(\eta c)}{\eta^2}+\frac{2}{\pi}\int_0^{\pi/2} w[c\sin\theta,t]\,\mathrm{d}\theta. \tag{15}$$

It is convenient to introduce a new unknown function $d(x,t)=\alpha w_t(x,t)+\varphi(x,0,t)$, $-1<x<1$, which makes it possible to rewrite the beam Equation (3) with account for (6) in the form

$$d_t+\beta w_{xxxx}=0, \tag{16}$$

$$\alpha w_t+\varphi(x,0,t)=d(x,t). \tag{17}$$

The boundary-value problem (16), (17), (4), (5), (7–10), (15) is solved with the help of the normal-mode method. This method leads to an infinite system of ordinary differential equations with respect to principal coordinates of the beam deflection $w(x,t)$, $-1<x<1$. Within the framework of the normal-mode method, the beam deflection $w(x,t)$ and the function $d(x,t)$ are sought in the forms

$$w(x,t)=\sum_{n=1}^{\infty} a_n(t)\psi_n(x), \tag{18}$$

$$d(x,t)=\beta\sum_{n=1}^{\infty}\lambda_n^4 d_n(t)\psi_n(x). \tag{19}$$

Here $\psi_n(x)$ are the non-trivial solutions of the homogeneous boundary-value problem

$$\frac{\mathrm{d}^4\psi_n}{\mathrm{d}x^4} = \lambda_n^4\psi_n \ (-1 < x < 1), \qquad \psi_n = \frac{\mathrm{d}^2\psi_n}{\mathrm{d}x^2} = 0 \ (x = \pm 1), \tag{20}$$

and λ_n are the corresponding eigenvalues. Moreover, the eigenfunctions $\psi_n(x)$ satisfy the orthogonality condition

$$\int_{-1}^{1} \psi_n(x)\,\psi_m(x)\,\mathrm{d}x = \delta_{nm}, \tag{21}$$

where $\delta_{nm} = 0$ for $n \neq m$ and $\delta_{nn} = 1$. In the case of a simply supported beam and central impact, the eigenfunctions $\psi_n(x)$ are given as $(n \geq 1)$

$$\psi_n(x) = \cos(\lambda_n x), \ \lambda_n = \pi(n - 1/2). \tag{22}$$

It is convenient to take the principal coordinates $a_n(t)$ of the beam deflection as the new unknown functions and to express other quantities with their help.

On the interval of the liquid boundary, $y = 0, -1 < x < 1$, which contains the contact region, $-c(t) < x < c(t), c(t) \leq 1$, the velocity potential can be presented as

$$\varphi(x, 0, t) = \sum_{n=1}^{\infty} b_n(t)\psi_n(x), \tag{23}$$

$$b_n(t) = \int_{-c(t)}^{c(t)} \varphi(x, 0, t)\psi_n(x)\,\mathrm{d}x.$$

This follows from Equations (17–19) and (8). In order to find the dependencies of the coefficients $b_m(t)$ on the principal coordinates $a_n(t)$, where $m, n \geq 1$, we must consider the hydrodynamic part (7–10) of the original problem. We introduce the harmonic in the lower half-plane functions $\varphi_n(x, y, c)$, which satisfy equations

$$\frac{\partial^2\varphi_n}{\partial x^2} + \frac{\partial^2\varphi_n}{\partial y^2} = 0 \ (y < 0),$$

$$\varphi_n = 0 \ (y = 0, \ |x| > c(t)),$$

$$\frac{\partial\varphi_n}{\partial y} = \psi_n(x) \ (y = 0, \ |x| < c(t)),$$

$$\varphi_n \to 0 \ (x^2 + y^2 \to \infty).$$

Here $n = 0, 1, 2, \ldots$ and $\psi_0(x) \equiv 1$. We obtain

$$\varphi(x, 0, t) = -\sqrt{c^2 - x^2} + \sum_{n=1}^{\infty} \dot{a}_n(t)\varphi_n(x, 0, c),$$

$$b_m(t) = -f_m(c) + \sum_{n=1}^{\infty} \dot{a}_n(t)S_{nm}(c), \tag{24}$$

$$f_m(c) = \int_{-c}^{c} \sqrt{c^2 - x^2}\psi_m(x)\,\mathrm{d}x, \qquad S_{nm}(c) = \int_{-c}^{c} \varphi_n(x, 0, c)\psi_m(x)\,\mathrm{d}x,$$

where a dot stands for the time derivatives. Green's second identity gives that the matrix S with the elements $S_{nm}(c)$, where $m, n = 1, 2, \ldots$, is symmetrical. Taking (22) into account, we

find [12]

$$f_m(c) = \pi c^2 J_1(\lambda_m c)/(\lambda_m c), \qquad S_{nn}(c) = \frac{\pi}{2} c^2 \left[J_0^2(\lambda_n c) + J_1^2(\lambda_n c) \right],$$

$$S_{nm}(c) = \frac{\pi c}{\lambda_n^2 - \lambda_m^2} \left[\lambda_n J_0(\lambda_m c) J_1(\lambda_n c) - \lambda_m J_0(\lambda_n c) J_1(\lambda_m c) \right] \ (n \neq m),$$

where $J_0(z)$ and $J_1(z)$ are the zero- and first-order Bessel functions.

Substituting (18), (19), (23) and (24) in (16), (17) and taking into account the orthogonality condition (21), we arrive at an infinite system of ordinary differential equations with respect to the principal coordinates

$$\frac{\mathrm{d}\vec{a}}{\mathrm{d}t} = (\alpha I + S)^{-1}(\beta D\vec{d} + \vec{f}), \tag{25}$$

$$\frac{\mathrm{d}\vec{d}}{\mathrm{d}t} = -\vec{a}. \tag{26}$$

Here $\vec{a} = (a_1, a_2, a_3, ...)^T, \vec{d} = (d_1, d_2, d_3, \dots)^T$, $\vec{f} = (f_1(c), f_2(c), f_3(c), \dots)^T$, I is the unit matrix and D is the diagonal matrix, $D = \mathrm{diag}\{\lambda_1^4, \lambda_2^4, \lambda_3^4, \dots\}$. The right-hand sides of system (25) and (26) depend on $\vec{a}$, $\vec{d}$ and c, but not on the time t, which is why it is convenient to take the quantity c as a new independent variable ($0 \le c \le 1$) instead of time t. Time t is a function of c now, $t = t(c)$. This substitution is justified under the condition $\mathrm{d}c/\mathrm{d}t > 0$, which follows from assumption (A10). A differential equation for the unknown function $t(c)$ can be obtained from Equation (15) after its differentiation with respect to c:

$$\frac{\mathrm{d}t}{\mathrm{d}c} = Q(c, \vec{a}, \dot{\vec{a}}), \tag{27}$$

$$Q(c, \vec{a}, \dot{\vec{a}}) = \frac{\eta^{-1} J_1(\eta c) + (2/\pi)(\vec{a}, \vec{\Gamma}_c(c))}{1 - (2/\pi)(\dot{\vec{a}}, \vec{\Gamma}(c))},$$

$$\Gamma_n(c) = \int_0^{\pi/2} \psi_n(c \sin\theta)\, \mathrm{d}\theta, \quad \vec{\Gamma}_c(c) = \mathrm{d}\vec{\Gamma}/\mathrm{d}c.$$

For a simply supported beam, we obtain $\Gamma_n(c) = (\pi/2) J_0(\lambda_n c)$ and $(\Gamma_c)_n = -(\pi \lambda_n/2) J_1(\lambda_n c)$.

Multiplying equations of system (25), (26) by $\mathrm{d}t/\mathrm{d}c$ and taking (27) into account, we find

$$\frac{\mathrm{d}\vec{a}}{\mathrm{d}c} = \vec{F}(c, \vec{d})\, Q(c, \vec{a}, \vec{F}(c, \vec{d})), \quad \frac{\mathrm{d}\vec{d}}{\mathrm{d}c} = -\vec{a}\, Q(c, \vec{a}, \vec{F}(c, \vec{d})), \tag{28}$$

where $\vec{F}(c, \vec{d}) = (\alpha I + S(c))^{-1}(\beta D\vec{d} + \vec{f}(c))$ and $\dot{\vec{a}} = \vec{F}(c, \vec{d})$. The initial conditions for system (27), (28) are

$$\vec{a} = 0, \quad \vec{d} = 0, \quad t = 0 \quad (c = 0). \tag{29}$$

The system (27), (28) is suitable for numerical evaluation of the hydroelastic behavior of the impacting beam. Indeed, for small times we have $c(t) = O(t^{1/2})$, $w(x, t) = O(t^{3/2})$, $w_t = O(t^{1/2})$, $w_{tt} = O(t^{-1/2})$. Therefore, one cannot start numerical calculations for system (25), (26) with zero initial conditions. Kvålsvold and Faltinsen [3] described the difficulties with initial conditions for a system of differential equations with respect to principal coordinates $a_n(t)$ and their derivatives $\dot{a}_n(t)$, where the time t is taken as the independent variable. On the other hand, $t = O(c^2)$, $w = O(c^3)$, $\vec{a} = O(c^3)$, $\mathrm{d}\vec{a}/\mathrm{d}c = O(c^2)$, $\vec{d} = O(c)$, $\mathrm{d}\vec{d}/\mathrm{d}c = O(1)$ as $c \to 0$, and, therefore there are no problems with initial conditions for system (27–28).

Details of the numerical analysis of the initial-value problem (27–29) are given in [12]. Estimation of the optimal step of integration Δc and its dependence on the number of modes taken into account were discussed.

In order to explain the present approach and outline its main features as compared with the classical approaches to the numerical analysis of water impact, we consider a simple initial-value problem

$$v_{tt} + v = t^{-1/2} \ (t > 0), \ v(0) = v_t(0) = 0. \tag{30}$$

The equation is similar to the beam Equation (3). It is worth noting that $p(0, 0, t) = O(t^{-1/2})$ as $t \to 0$ in (3) [17]. The standard approach is based on the decomposition of (30) as

$$v_t = u(t), \ u_t = -v + t^{-1/2}, \quad v(0) = 0, \ u(0) = 0.$$

The right-hand side of this ordinary differential system is singular as $t \to 0$ (compare with system (25)). This is the main difficulty for starting the numerical procedure. There are three possible ways to overcome this difficulty: (1) resolve the singularity of the forced term, $t^{-1/2}$, from a physical point of view [6]; (2) obtain asymptotics of the solution as $t \to 0$ and start the numerical simulation from that approximate solution at $t = t_\epsilon$, where $0 < t_\epsilon \ll 1$ [18]; (3) use another decomposition (see below).

Equation (30) can be rewritten in the form

$$(v_t - 2t^{1/2})_t' + v = 0,$$

which leads to another way of decomposing the problem

$$v_t = q(t) + 2t^{1/2}, \quad q_t = -v, \quad v(0) = q(0) = 0, \tag{31}$$

which the present approach is based on (the function $q(t)$ is equivalent to the function $d(x, t)$ introduced in (16), (17)). The initial problem (31) is already suitable for numerical analysis. However, higher derivatives of the solution are singular at $t = 0$. This may lead to loss of accuracy for small t. This is a reason for introducing new independent variable, $\tau = t^{1/2}$, with the help of which problem (31) can be rewritten as

$$v_\tau = 2\tau a(t) + 4\tau^2, \ a_\tau = -2\tau v(\tau), \quad v(0) = a(0) = 0. \tag{32}$$

This change of the independent variable is equivalent to the replacement of time t for c in system (28). The right-hand side of system (32) is analytic with respect to the independent variable τ and the unknown functions $v(\tau)$ and $a(\tau)$. This implies that the solution is also an analytical function of τ and can be readily computed.

4. Edge impact

It was shown by Kvålsvold and Faltinsen [4] that wave impact on the bow part of the wetdeck of a catamaran is possible and that this phenomenon needs particular attention. In Section 2 it was also pointed out that the edge-impact problem corresponds to the second phase of an elastic plate impact and its solution has to be incorporated into the computer code to treat the impact under arbitrary conditions. Theoretical analysis of the edge-impact problem was given by Korobkin [19] within a one-mode approximation and by Korobkin and Khabakhpasheva [16] using the normal-mode method.

In the case of edge impact (Figure 3) the liquid flow and the plate deflection are governed by the boundary-value problem (3–10), where $D=\{x \mid 0<x<c_2(t)\}$ and $x_1=0$ in (11). The modified Wagner condition (14) has to be replaced by (see [19])

$$\int_0^{\pi/2} \sin^2\theta\, y_b[c_2(t)\sin^2\theta, t]\,\mathrm{d}\theta = 0, \tag{33}$$

which, with account taken for (11), provides

$$t=\frac{1-g(\eta c_2)}{\eta^2}+\frac{4}{\pi}\int_0^{\pi/2}\sin^2\theta\, w[c_2\sin^2\theta, t]\,\mathrm{d}\theta,$$

where

$$g(z)=\int_0^1 \frac{\sqrt{\sigma}\cos(z\sigma)}{\sqrt{1-\sigma}}\,\mathrm{d}\sigma.$$

We use the same decomposition of the beam equation as in Section 3. The plate deflection $w(x,t)$ and the function $d(x,t)$ are sought in forms (18) and (19), where now $\psi_n(x)=\sin(\lambda_n x)$, $\lambda_n=\pi n/2$, $n=1,2,\ldots$ and $0<x<2$. Representations of the velocity potential (23), (24) have to be replaced by (see [16])

$$\varphi(x,0,t)=\sum_{n=1}^{\infty} b_n(t)\psi_n(x)\ \ (0<x<2), \qquad b_m(t)=-f_m(c_2)+\sum_{n=1}^{\infty}\dot{a}_n(t)S_{nm}(c_2),$$

$$f_m(c_2)=\frac{\pi c_2\sin(\lambda_m c_2/2)}{2\lambda_m}v_m,$$

$$S_{nm}(c_2)=\frac{c_2}{2\pi\lambda_m}\left[\cos\frac{\lambda_m c_2}{2}\cos\frac{\lambda_n c_2}{2}S_{nm}^{(1)}(c_2)-\sin\frac{\lambda_m c_2}{2}\sin\frac{\lambda_n c_2}{2}S_{nm}^{(2)}(c_2)\right], \tag{34}$$

$$S_{nm}^{(1)}=-\pi^2 u_m v_n-\frac{\pi^2\lambda_m}{(\lambda_n^2-\lambda_m^2)}[\lambda_m u_m v_n-\lambda_n u_n v_m], \qquad S_{nn}^{(1)}=-\pi^2 u_n v_n-S_{nn}^{(2)},$$

$$S_{nm}^{(2)}=\frac{\pi^2\lambda_m}{(\lambda_n^2-\lambda_m^2)}[\lambda_m v_m u_n-\lambda_n v_n u_m], \qquad S_{nn}^{(2)}=-\frac{\pi^2\lambda_n c_2}{4}\left[u_n^2+v_n^2\right],$$

$$u_m=J_0\left(\frac{\lambda_m c_2}{2}\right), \qquad v_m=J_1\left(\frac{\lambda_m c_2}{2}\right).$$

By taking (33) and (34) into account, we arrive at systems (25–26) and (27–28), where the function $Q(c_2,\vec{a},\dot{\vec{a}})$ is obtained now by differentiation of (33) with respect to c_2.

The initial-value problem (27–29) in the case of edge impact, where the elements of the system are given by (34), is solved numerically by the Runge–Kutta method. This approach is only valid when the velocity of the contact region expansion $\mathrm{d}c_2/\mathrm{d}t$ is positive and finite. If the velocity vanishes and becomes negative, the liquid particles from the contact region escape onto the liquid free surface, and a vortex layer, which is ignored in the present model, is formed. If the velocity grows and becomes comparable to the sound velocity in the liquid, acoustic effects must be taken into account. Therefore, in general, the parameter plane (α,β) is divided into three parts (Figure 6): (1) $\mathrm{d}c_2/\mathrm{d}t$ becomes negative with time; (2) $\mathrm{d}c_2/\mathrm{d}t$ is unbounded; (3) $\mathrm{d}c_2/\mathrm{d}t$ is positive and finite during the impact stage. It is seen that the Wagner approach should be modified for very flexible beams with small β. It is well-known that the total hydrodynamic force grows beyond all bounds as $\mathrm{d}c_2/\mathrm{d}t\to+\infty$. This phenomenon is referred to as blockage. In this

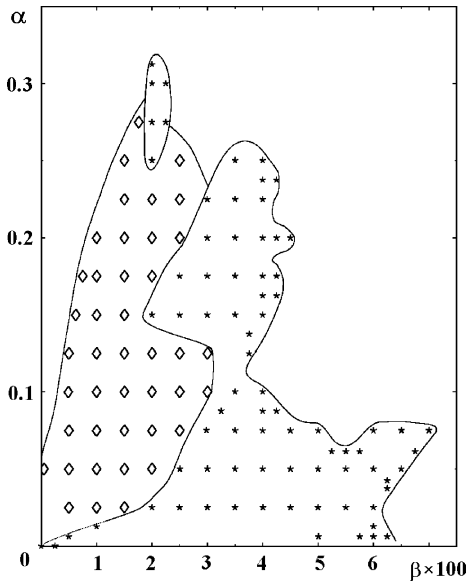

Figure 6. Plane of parameters α, β. The regions, where $dc_2/dt < 0$(◇) and where dc_2/dt is unbounded (⋆), are distinguished. The Wagner approach is only valid outside these two regions.

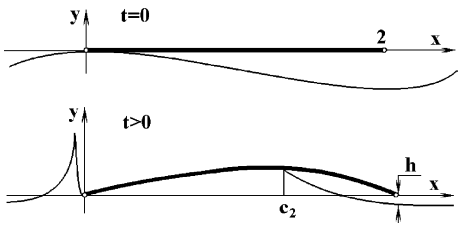

Figure 7. Blockage phenomenon.

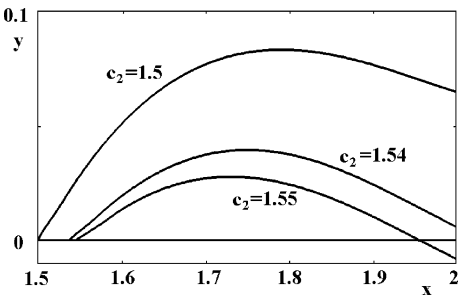

Figure 8. Distance between the elastic plate and the disturbed liquid free surface at different time instants ($c_2 < x < 2$).

case the rate of the added-mass increase is very high, which is mainly due to the elastic deflection of the beam. This result is of practical importance because it indicates that flexibility of impacting surfaces may lead to hydrodynamic loads that are greater than those for equivalent rigid surfaces.

Analysis of the blockage phenomenon shows that the liquid flow may be more complicated than predicted by the Wagner theory. Namely, the right edge of the plate may enter the disturbed liquid free surface before the velocity of the contact point becomes very high (Figure 7). The distance between the right edge of the beam and the disturbed free surface is shown in Figure 8 for $\alpha = 0{\cdot}157$, $\beta = 0{\cdot}0294$ as a function of the contact-region dimension c_2. If the blockage phenomenon has been detected in numerical calculations, cavity formation near the right edge of the beam is expected. The presence of the air in the cavity may essentially change the process of the plate–liquid interaction. This problem is not considered here. The blockage was not observed in the central-impact case, which means that the impact conditions are responsible for this phenomenon.

Comparison between edge impact (curves 2) and central impact (curves 1) is presented in Figure 9. Distributions of the beam deflection, velocity of the beam elements and the bending stresses along the beam are shown at the end of the impact stage. The impact conditions in both cases are identical, except for the impact-point position. Curves 1 are symmetrical with respect to the beam centre, $x = 1$. Calculations were performed for $\alpha = 0{\cdot}314$ and $\beta = 0{\cdot}311$, which corresponds to the impact of an elastic plate onto a wave crest with a radius of curvature of $R = 10$ m. The plate of length 1m and thickness 2 cm is made of mild steel and hits the waves at velocity 3 m/s. In dimensional variables, the duration of the impact stage is 0·36 for the central impact and 1·537 for edge impact. It is seen that the increase of the impact-stage duration leads to a more than double increase of the deflection amplitude, a significant decrease in the kinetic energy of the beam and an increase in the potential energy of the deformed beam. Figure 9 demonstrates that the position of the impact point has a strong effect on beam behavior at the end of the impact stage, with other impact conditions being identical.

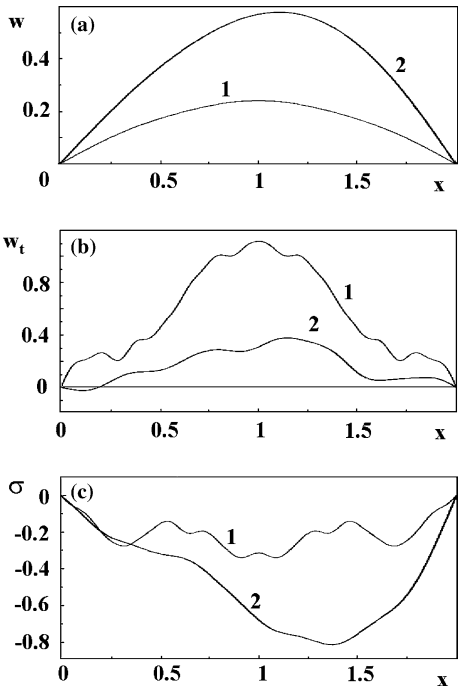

Figure 9. Distributions of the beam deflection (a), beam velocity (b), and the bending stresses (c) along the beam at the end of the impact stage for central impact (curves 1) and edge impact (curves 2).

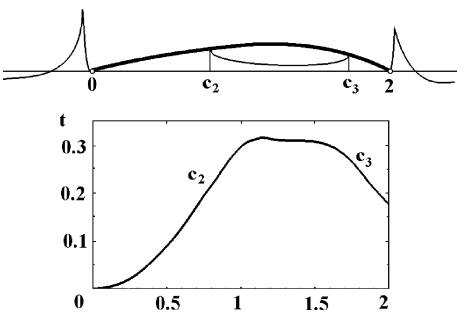

Figure 10. Trajectories of the contact points.

5. Impact with attached cavity

The interaction between an elastic plate and the liquid during the third part of the impact stage, $t_2 < t < t_3$, is governed by the boundary-value problem (3–10), where $D = \{x \mid 0 < x < c_2(t),\ c_3(t) < x < 2\}$ (Figure 4). The initial conditions are given by (12) at $t = t_2$. The presence of air in the cavity, $y = 0, c_2(t) < x < c_3(t)$, is neglected. We consider only the case, where $\mathrm{d}c_2/\mathrm{d}t > 0$ and $\mathrm{d}c_3/\mathrm{d}t < 0$. Formulae (16–21) are still valid and the eigenfunctions $\psi_n(x)$ are the same as in the edge-impact problem (see Section 4).

In order to derive equations for the functions $c_2(t), c_3(t)$, we consider the vertical displacement of the liquid free surface [21]

$$Y(x,0,t) = \frac{1}{\pi W(x)}\left(\int_0^{c_2} \frac{y_b(\tau,t)W(\tau)}{\tau - x}\mathrm{d}\tau - \int_{c_3}^{2} \frac{y_b(\tau,t)W(\tau)}{\tau - x}\mathrm{d}\tau + F(t)\right), \tag{35}$$

where $x \notin D(t)$. The characteristic function $W(x)$ of the contact region is given as

$$W(x) = \sqrt{x(x-c_2)(c_3-x)(2-x)},$$

and $F(t)$ is an arbitrary function of time. The vertical displacement $Y(x,0,t)$ is bounded at the contact points $x = c_2$ and $x = c_3$ if and only if

$$\int_0^{c_2} y_b(\tau,t)\sqrt{\frac{\tau(2-\tau)}{(c_2-\tau)(c_3-\tau)}}\mathrm{d}\tau - \int_{c_3}^{2} y_b(\tau,t)\sqrt{\frac{\tau(2-\tau)}{(\tau-c_2)(\tau-c_3)}}\mathrm{d}\tau = 0,$$

$$\int_0^{c_2} y_b(\tau,t)\sqrt{\frac{\tau(2-\tau)(c_3-\tau)}{c_2-\tau}}\mathrm{d}\tau+\int_{c_3}^{2} y_b(\tau,t)\sqrt{\frac{\tau(2-\tau)(\tau-c_3)}{\tau-c_2}}\mathrm{d}\tau=F(t).$$

Differentiation of these equations with respect to time leads to the following system for the derivatives $\dot{c}_2$ and $\dot{c}_3$

$$a_{11}\dot{c}_2+a_{12}\dot{c}_3=b_1,\quad a_{21}\dot{c}_2+a_{22}\dot{c}_3=b_2+\dot{F}(t), \tag{36}$$

the initial conditions for which are

$$c_2(t_2)=c_2(t_2-0),\ c_3(t_2)=2. \tag{37}$$

Here $a_{11}, a_{12}, a_{21}, a_{22}, b_1$ and b_2 are given functions of c_2, c_3 and t. The vertical velocity of the liquid free surface is given by

$$\varphi_y(x,0,t)=\frac{1}{\pi W(x)}\left(\int_0^{c_2}\frac{\varphi_y(\tau,t)W(\tau)}{\tau-x}\mathrm{d}\tau-\int_{c_3}^{2}\frac{\varphi_y(\tau,t)W(\tau)}{\tau-x}\mathrm{d}\tau+C(t)\right), \tag{38}$$

where $x\notin D(t)$ and $\varphi_y(\tau,0,t)=-1+w_t(\tau,t)$. Far from the contact region, $x\to+\infty, y=0$, Equations (35) and (38) provide

$$Y(x,0,t)\sim\frac{F(t)}{\pi x^2},\quad \varphi_y(x,0,t)\sim\frac{C(t)}{\pi x^2},$$

which, with account taken for the equality $Y_t=\varphi_y$, yield the equation

$$\frac{\mathrm{d}F}{\mathrm{d}t}=C(t). \tag{39}$$

The function $C(t)$ is determined from the condition $\varphi(c_3,0,t)=0$, which is used in the following form

$$\int_{c_3}^{2}\varphi_x(x,0,t)\mathrm{d}x=0, \tag{40}$$

where

$$\frac{\partial\varphi}{\partial x}(x,0,t)=-\frac{1}{\pi W(x)}\left(\int_0^{c_2}\frac{W(\tau)\varphi_y(\tau,0,t)}{\tau-x}\,\mathrm{d}\tau-\mathbf{P.v.}\int_{c_3}^{2}\frac{W(\tau)\varphi_y(\tau,0,t)}{\tau-x}\,\mathrm{d}\tau+C(t)\right).$$

The integrals in Equations (36) and (40) are transformed into forms that are suitable for their numerical evaluation by Simpson's rule.

The principal coordinates $a_n(t)$ are governed by the system of ordinary differential Equations (25–26), (36) and (39), where now $(n\geq 1)$

$$f_m=S_{0m}(c_2,c_3),\ \psi_0(x)=1,\ \psi_n(x)=\sin\lambda_n x,$$
$$S_{nm}(c_2,c_3)=\frac{1}{\lambda_m}\left(\int_0^{c_2}\cos(\lambda_m x)\frac{\partial\varphi_n}{\partial x}\mathrm{d}x+\int_{c_3}^{2}\cos(\lambda_m x)\frac{\partial\varphi_n}{\partial x}\mathrm{d}x\right), \tag{41}$$

and

$$\frac{\partial\varphi_n}{\partial x}=\frac{1}{\pi W(x)}\left(\mathbf{P.v.}\int_0^{c_2}\frac{W(\tau)\psi_n(\tau)}{\tau-x}\mathrm{d}\tau-\int_{c_3}^{2}\frac{W(\tau)\psi_n(\tau)}{\tau-x}\mathrm{d}\tau+C_n\right)\ (0<x<c_2),$$
$$\frac{\partial\varphi_n}{\partial x}(x,0,t)=-\frac{1}{\pi W(x)}\left(\int_0^{c_2}\frac{W(\tau)\psi_n(\tau)}{\tau-x}\,\mathrm{d}\tau-\mathbf{P.v.}\int_{c_3}^{2}\frac{W(\tau)\psi_n(\tau)}{\tau-x}\,\mathrm{d}\tau+C_n\right)\ (c_3<x<2),$$

where the constants C_n are numerically determined by using condition (40). The integrals in (41) are evaluated numerically by Simpson's rule.

Numerical calculations were performed with 5 and 10 elastic modes for two cases. In the first case the wave profile was approximated by a parabolic contour ($\eta \to 0$), and in the second case was given by Equation (1). It was revealed that, even in the first case, the air can be trapped close to the right edge of the impacting plate ($\alpha = 0{\cdot}157$ and $\beta = 0{\cdot}03$). After the cavity has been formed, the contact points are accelerated. The cavity is very thin and exists for a short period. The hydrodynamic pressures during the collapse of the cavity are very high but of short duration. In fact, "secondary" hydrodynamic impact onto the plate occurs with loads being much higher than at the beginning of the plate–liquid interaction. It should be noted that the deflections change just a little during the third phase. However, the high pressures affect the bending stresses, which grow significantly.

It was found that the value t_2, which has to be determined together with the liquid flow and the beam deflection, must be evaluated very precisely to make the numerical scheme stable. It was proved that system (36) provides $(\mathrm{d}c_3/\mathrm{d}t)(t_2) = 0$. This equality is used to start the simulation of the plate/liquid interaction during the third phase.

In the second series of calculations the initial shape of the liquid free surface is given by (11) in non-dimensional variables with $\eta = 3\pi/4$, which implies that the wave length is 4/3 of the total plate length, and $\alpha = 0{\cdot}248$, $\beta = 0{\cdot}0573$. This corresponds to the experimental conditions [1]: the steel plate of thickness 8 mm and length 0·5 m falls from a height of 1 m against regular waves with the radius of curvature at the wave crest equal to 10 m. It was taken that $x_1 = 0$. During the impact stage a cavity is formed due to the geometry of the initial shape of the liquid surface. The cavity size and the duration of the third stage are much greater than in the first case. The trajectories of the contact points are shown in Figure 10. Bending stresses and deflections vary smoothly during the third phase in the present case.

6. Penetration stage

During the penetration stage the beam is totally wetted but continues to interact with the liquid. The process is described by the boundary-value problem (3–10), where $D = (0, 2)$ and the initial conditions (5) have to be changed as follows

$$w(x, t_3) = w(x, t_3 - 0), \;\; w_t(x, t_3) = w_t(x, t_3 - 0), \tag{42}$$

where $w(x, t_3 - 0)$ and $w_t(x, t_3 - 0)$ are the beam deflection and the beam velocity, respectively, at the end of the impact stage. This problem is equivalent to that of a floating elastic plate, which starts to enter the liquid at $t = t_3$ with a constant velocity and both the initial deflection of the plate and the initial velocity of its elements being prescribed. A theoretical analysis of this stage was given by Faltinsen [7]; see also [14]. In the last paper the problem is formulated with respect to the hydrodynamic pressure $p(x, y, t)$ and the beam deflection $w(x, t)$. The scales of time and of the unknown functions are chosen in accordance with recommendations by Faltinsen [7]. The beam deflection is sought as a superposition of eigenfunctions of the spectral problem for a totally wetted elastic plate. Details of the analysis of "wet" modes and formulae for the elements of the matrix of hydrodynamic coefficients S_{nm} (see (25)) can be found in [14]. It was found that the first "dry" and "wet" modes are practically identical, for the second modes the difference is less than 8%, for the third modes less than 7% and for the fourth modes less than 6%. Therefore, it is reasonable to use "dry" modes, the shapes of which are given analytically, to describe the beam deflection during the penetration stage. The

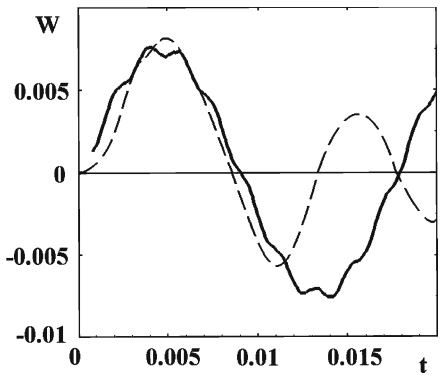

Figure 11. Deflection of the beam centre. *Solid line*: calculations; *broken line*: experiments.

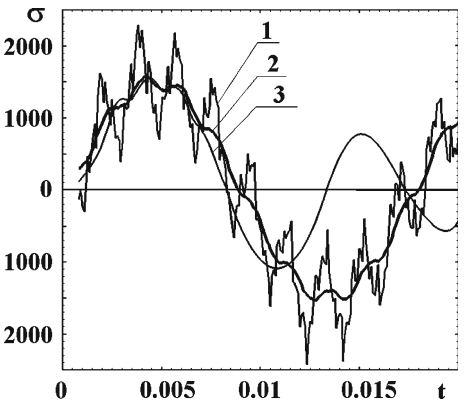

Figure 12. The strains (in μs) at the beam centre as a function of the time (in seconds) during the penetration stage. Direct computations (*curve 1*), average stresses (*curve 2*), experiments (*curve 3*).

eigenfunctions and the corresponding eigenvalues for totally wetted elastic plate are dependent on the parameter α but not on β.

Calculations were performed for $\alpha = 0{\cdot}252$ and spring conditions at the beam edges [2]

$$w'' = 0, \qquad \frac{\partial^2 w}{\partial x^2} \pm k \frac{\partial w}{\partial x} = 0 \qquad (x = 0 \text{ and } x = 2), \tag{43}$$

where plus is for $x = 2$ and minus for $x = 0$, k is the nondimensional rigidity of the spring. A value of $k = 2{\cdot}85$ was taken in the present calculations.

It should be noted that the numerical analysis of the plate/liquid interaction during the penetration stage does not require a special treatment of the original boundary-value problem and can be performed with the help of the numerical scheme described in Section 4 for the edge-impact case. We need only to omit Equation (33) because $c_2 \equiv 2$ at the penetration stage and to replace c_2 in (34) by 2. Both the matrix S and the vector $\vec{f}$ do not depend on time now and system (25), (26) can be readily integrated numerically.

Within the experimental conditions ($\alpha = 0{\cdot}2512, \beta = 0{\cdot}0551, k = 2{\cdot}85$) the calculations were performed with 15 dry modes for problem (3), (6–10), (42) and (43) in the case of central impact. A comparison between experimental and numerical results is shown in Figure 11 for the plate deflection and in Figure 12 for the amplitude of bending stresses at the beam center point, $x = 1$. The convergence of the series for the strain has been investigated. If more than 15 modes are used, additional small-amplitude vibrations appear. The amplitude is so small that the vibrations are difficult to recognize on the graph. It should be noticed that the distribution of strain along the beam is rather smooth at any time instant (see Figure 9c, for example).

The predicted deflection at the plate midpoint corresponds fairly well to the measured deflection at this point (see also the comparison in [2]). Predicted stresses clearly overestimate contributions of higher modes, which are suppressed in the experimental results. A similar overestimation can be found in the theoretical results of Faltinsen *et al.* [2], which were obtained by using the same model but with simplified initial conditions

$$w(x, t_3) = 0, \qquad w_t(x, t_3) = 1.$$

An explanation of the higher-mode generation during the plate impact is given in Section 7. However, there is a simple possible explanation based on an analysis of the parameters of the stress

gauges used in the experiments. Resonance frequencies of the stress gauges are not reported in [2]. We use the data reported in [22]. In [22] the hydroelastic behavior of a circular elastic cylinder was studied with the help of the stress gauges having a resonance frequency of 5 kHz. If we assume that the resonance frequency of the stress gauges in the Norwegian experiments is equal to 3 kHz, we may average the numerical results over the time interval $2{\cdot}25 \times 10^{-3}$ s. Averaged numerical stresses (curve 2) fit the experimental ones fairly well (see Figure 12).

7. Generation of higher modes

There are several reasons for higher modes to be generated during the impact stage. These are: (1) initially very high hydrodynamic pressures are localized close to the impact point; (2) pressure distribution along the wetted part of the plate is highly non-uniform and is unbounded at the moving contact points; (3) the area, along which the hydrodynamic loads act, grows with time. Calculations were performed to demonstrate that the third reason, which is the main feature of the impact stage, is responsible for the generation of higher modes.

We consider the edge-impact problem ($\alpha = 0{\cdot}247$, $\beta = 0{\cdot}05733$, $\eta = \pi/6$) for a simply supported beam. The non-dimensional stress amplitude is given by

$$\sigma(x,t) = \sum_{n=1}^{\infty} \sigma_n(t)\psi_n(x),$$

where $\psi_n(x) = \sin(\lambda_n x)$, $\lambda_n = \pi n/2$, $\sigma_n(t) = -a_n(t)\lambda_n^2/2$ and $a_n(t)$ are the principal coordinates of the beam deflection. The functions $\sigma_n(c_2)$, $n = 1, 2, 3, 4$, $0 < c_2 < 2$, where c_2 is the contact-region dimension, are shown in Figure 13 together with the shapes of the corresponding modes. It is seen that $\sigma_1(c_2)$ is a monotonic function, and that $\sigma_2(c_2)$ peaks at the instant when the contact point passes the node of the second mode. Correspondingly, the amplitude of the contribution of the third mode to the bending stresses, $\sigma_3(c_2)$, peaks at the instant when the

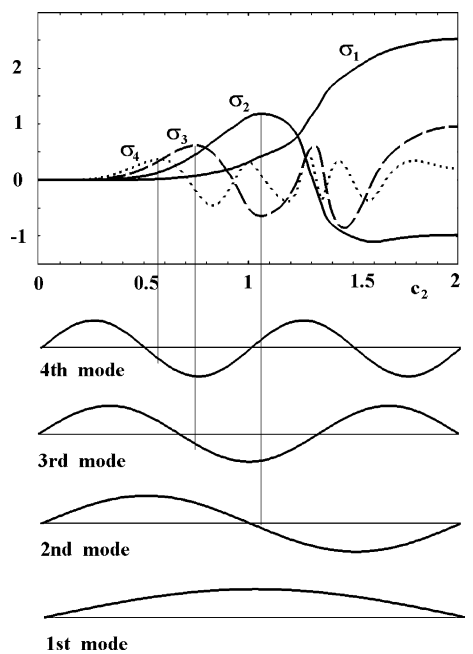

Figure 13. Contributions of normal modes to the bending stresses.

contact point passes the first node of the third mode, and so on. After their first peaks the functions $\sigma_n(c_2)$ do not grow essentially. The magnitudes of the peaks decrease monotonically as the number n increases. We may conclude that the highest modes are generated just after the impact instant and are influenced by fine details of the flow at the very beginning of the impact, but their amplitudes are rather small. The modes with moderate numbers are generated much later and their amplitudes are affected by the velocity of the expansion of the contact region. The first mode does not reach its maximum at the impact stage. This preliminary analysis makes it possible to believe that a correct description of high-mode contributions to the bending stresses is connected neither with fine details of the very initial stage of the impact, when the speed of the contact point is very high and acoustic effects have to be taken into account, nor with fine details of the pressure distribution close to the contact points, where nonlinear effects are of importance, but with the effect of moving the load.

We may assume that the amplitudes of the higher modes decay during the penetration stage due to sound radiation. Indeed, the period of the second "dry" mode for the plate used in the experiments [1] (but simply supported) is 0·00125 s; the scale of acoustic effects is of the order 0·0003 s (this time scale is equal to the initial length of the beam 0·5 m divided by the sound velocity 1500 m/s) and the bending stresses reach their maximum values at 0·005s approximately. Taking into account that the acoustic radiation of energy is more intensive for higher frequencies than for lower ones, we may conclude that acoustic effects may be responsible for suppressing the higher modes well before the stresses reach their maximum.

8. Global characteristics of the impact stage

Previous sections of this paper show that the interaction between an elastic plate and a liquid can be very complicated during the impact stage. On the other hand, assuming that the maximum bending stresses occur at the penetration stage, we need only to determine the plate deflection and its velocity at the end of the impact stage in order to evaluate the maximum amplitude of the bending stresses in the plate within Wagner's theory. This means that we need to obtain initial conditions to start numerical calculations for the penetration stage, during which the bending stresses approach their maximum values. According to the algorithm described in Sections 3–5 several possibilities of the process development have to be considered, which are essentially dependent on the initial shape of the liquid free surface. However, both the position of the free surface at the impact instant and this instant itself are not usually well-defined in practice. This means that one may expect only to obtain estimations of the bending-stress maximum, which is of primary practical interest, for a certain range of impact conditions but not the stress values themselves. If so, we shall study quantities, which are weakly dependent on the impact conditions, and use them to estimate maximum bending stresses. An experimental analysis of the dependence of the maximum stresses on the impact conditions (place of the impact, radius of the curvature at the wave crest) was given by Faltinsen *et al*. [2]. But the maximum of bending stresses is a local characteristic, which is why in theory it is not easy to estimate this quantity directly. We use another approach based on estimates of global characteristics (kinetic energy of the liquid flow, kinetic energy of the beam deflection and potential energy of the deformed plate), which are much easier to obtain. It is shown in this section that the global characteristics strongly depend on the impact conditions (this is clear from Figure 9) but the total energy of the plate–liquid system is highly conservative and is mainly dependent on the impact velocity and the plate parameters. In order to determine the global characteristics under consideration, we use the energy-conservation law for nonlinear liquid flow and linear elasticity of the beam. This point is very important,

because the correct result can not be derived within the linear theory of liquid flow, which is used for numerical simulations of the impact. The reason is that the energy-conservation law has to include the kinetic energy of spray jets, which is of the same order of magnitude as the kinetic energy of the main flow [23], but the spray jets are neglected within the Wagner approach used in this paper.

The kinetic energy of the nonlinear liquid flow (a prime stands for dimensional variables)

$$T_L^{'}(t') = \frac{1}{2}\rho \iint\limits_{\Omega(t')} (\nabla'\varphi')^2 \,\mathrm{d}x'\mathrm{d}y', \tag{44}$$

where ρ is the liquid density, $\Omega(t')$ is the flow region and $\varphi'(x', y', t')$ is the velocity potential of the nonlinear flow, is equal to the external work done to generate the flow

$$T_L^{'}(t') = -\int_0^{t'} \left(\int\limits_{D(\tau')} p' \frac{\partial \varphi'}{\partial y'} \mathrm{d}y' \right) \mathrm{d}\tau', \tag{45}$$

which follows from the energy conservation law for the liquid motion. Here $D(\tau')$ is the contact region between the entering elastic plate and the liquid at the instant τ'. It should be noted that, owing to its flexibility, the change of the plate shape is not taken into account in Equation (45). This approximation comes from the assumption that the amplitude of elastic plate deflections is small compared to both the plate length and the dimension of the contact region and gives a negligibly small contribution to the liquid flow. The interaction between the liquid and the entering elastic plate is mainly due to a decrease of the impact velocity

$$\frac{\partial \varphi'}{\partial y'} = -V + \frac{\partial w'}{\partial t'}(x', t') \tag{46}$$

but not due to variation of the plate shape.

Multiplying the beam Equation (3) rewritten in dimensional variables by $\partial w'/\partial t'$ and integrating the result along the plate and in time with the edge conditions (4) accounted, for we obtain

$$T_B^{'}(t') + P_B^{'}(t') = \int_0^{t'} \left(\int\limits_{D(\tau')} p' \frac{\partial w'}{\partial t'} \,\mathrm{d}x' \right) \mathrm{d}\tau', \tag{47}$$

where $T_B^{'}(t')$ is the beam kinetic energy,

$$T_B^{'}(t') = \frac{1}{2} M_B \int_0^{2L} \left(\frac{\partial w'}{\partial t'} \right)^2 (x', t') \,\mathrm{d}x', \tag{48}$$

and $P_B^{'}(t')$ is the potential energy of the deformed plate,

$$P_B^{'}(t') = \frac{1}{2} EJ \int_0^{2L} \left(\frac{\partial^2 w'}{\partial x'^2} \right)^2 (x', t') \,\mathrm{d}x'. \tag{49}$$

The left-hand side of the energy-conservation law for the elastic plate (47) will be more complicated for beam equations different from that of Euler and/or different edge conditions.

Combining Equations (45) and (47) and taking (46) into account, we find

$$T_B^{'}(t') + P_B^{'}(t') + T_L^{'}(t') = V \int_0^{t'} F^{'}(\tau') \,\mathrm{d}\tau',$$

where $F^{'}(t')$ is the total hydrodynamic force on the plate. In dimensionless variables the latter equation takes the form

$$T_B(t)+P_B(t)+T_L(t)=2\int_0^t F(\tau)\,\mathrm{d}\tau \tag{50}$$

with the quantities $\frac{1}{2}\rho V^2L^2$ and ρV^2R being the energy scale and the force scale, respectively.

The kinetic energy of the liquid flow can be approximately decomposed as $T_L=T_{LM}+T_{\mathrm{jet}}$, where $T_{LM}(t)$ is the energy of the main flow and $T_{\mathrm{jet}}(t)$ is the kinetic energy of the spray jets. The energy $T_{LM}(t)$ can be determined within the Wagner theory with $\Omega(t)$ being approximated by the lower half-plane $y\le 0$. The velocity potential $\varphi(x,y,t)$ is decomposed as

$$\varphi(x,y,t)=\varphi_R(x,y,t)+\varphi_E(x,y,t),$$

where $\varphi_R(x,y,t)$ satisfies Equations (7–10) with $w\equiv 0$ and $\varphi_E(x,y,t)$ satisfies the same equations but with condition (9) being replaced by $\partial\varphi_E/\partial y=w_t(x,t)$. The potential $\varphi_R(x,y,t)$ can be referred to as the velocity potential of the flow caused by rigid motion of the plate and $\varphi_E(x,y,t)$ as the velocity potential of the flow generated by the elastic deflection of the plate. It should be noted that both potentials depend on the geometry of the real contact region $D(t)$. We find

$$T_{LM}(t)\approx\iint\limits_{y<0}(\nabla\varphi)^2\,\mathrm{d}x\mathrm{d}y=\int\limits_{D(t)}\varphi_R\frac{\partial\varphi_R}{\partial y}\,\mathrm{d}x+2\int\limits_{D(t)}\varphi_E\frac{\partial\varphi_R}{\partial y}\,\mathrm{d}x+\int\limits_{D(t)}\varphi_E\frac{\partial\varphi_E}{\partial y}\,\mathrm{d}x. \tag{51}$$

On the other hand,

$$2\int_0^t F(\tau)\,\mathrm{d}\tau=2\int_0^2\int_0^t(-\varphi_t(x,0,\tau))\,\mathrm{d}\tau\mathrm{d}x=-2\int_0^2\varphi_R(x,0,t)\,\mathrm{d}x-2\int_0^2\varphi_E(x,0,t)\,\mathrm{d}x. \tag{52}$$

Substituting (51) and (52) in (50) and taking into account the equalities $(\partial\varphi_R/\partial y)(x,0,t)=-1$, where $x\in D(t)$, and $\varphi_R(x,0,t)=\varphi_E(x,0,t)=0$, where $x\notin D(t)$, we obtain

$$T_B(t)+P_B(t)+T_{LE}(t)\approx T_{LR}(t)-T_{\mathrm{jet}}(t). \tag{53}$$

Here

$$T_{LE}(t)=\int\limits_{D(t)}\varphi_E\frac{\partial\varphi_E}{\partial y}\,\mathrm{d}x,\qquad T_{LR}(t)=\int\limits_{D(t)}\varphi_R\frac{\partial\varphi_R}{\partial y}\,\mathrm{d}x.$$

The kinetic energy of the spray jets, $T_{\mathrm{jet}}(t)$, grows with time during the impact stage and is constant at the penetration stage because the jets are separated from the main flow region at $t=t_3$. The total energy of the jets at the penetration stage, $T_{\mathrm{jet}}(t_3)$, is denoted by T^*_{jet}. The kinetic energy $T_{LR}(t)$ grows during the impact stage and is equal to $\pi/2$ at the end of the impact stage and keeps this value thereafter.

It is worth noting that for an equivalent rigid plate the left-hand side in (53) is zero and we obtain the well-known result $T_{LR}(t)\approx T_{\mathrm{jet}}(t)$, which implies that the kinetic energy of spray jets is equal to the kinetic energy of the main flow during the impact stage [23].

The sum on the left-hand side of Equation (53) is referred to as the total elastic energy of the plate–liquid system and is denoted by $U(t)$. It is clear that the elastic energy is approximately constant

$$U(t)\approx\frac{\pi}{2}-T^*_{\mathrm{jet}}$$

during the penetration stage, $t>t_3$. We denote $U(t_3)$ by U_* and notice that

$$U_*\le\pi/2. \tag{54}$$

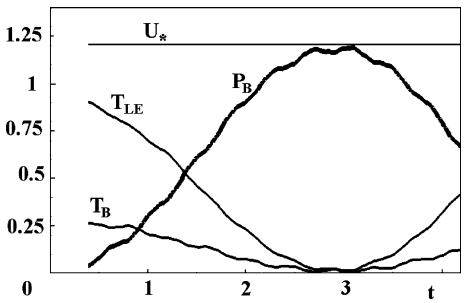

Figure 14. Components of the 'elastic' energy U_* as functions of time during the penetration stage.

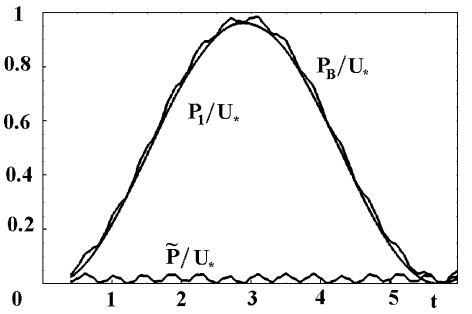

Figure 16. Relative contributions to the 'elastic' energy U_* of the total potential energy, P_B/U_*; the potential energy due to the first mode, P_1/U_*; the potential energy due to the modes from second to tenth, $\tilde{P}/U_*$.

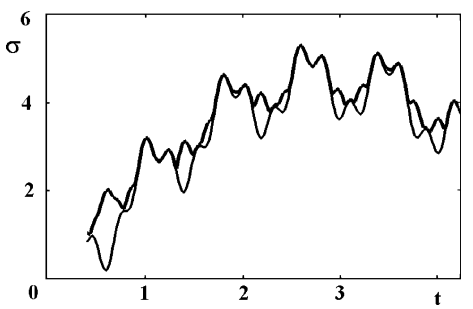

Figure 15. Evolution of the non-dimensional stresses in the plate during the penetration stage: *thick line* is for maximum stresses, *thin line* is for the bending stress at the plate centre.

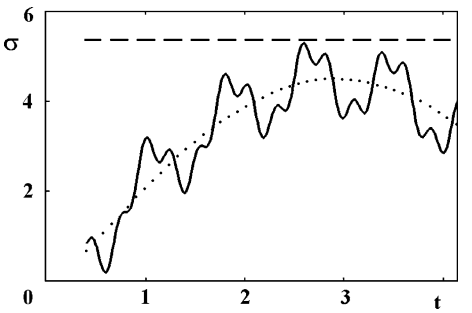

Figure 17. Non-dimensional stresses at the plate centre during the penetration stage: the solid line is for calculated bending stresses, the broken line is the theoretical estimation of the bending stresses, the dotted line is for bending stresses given by the one-mode approximation.

The dependence of U_* on impact conditions was studied numerically for $\eta = 3\pi/4$ and the steel plate used in the Norwegian experiments. It was revealed that U_* weakly depends on the impact location, $U_* \approx 1{\cdot}27$ for $0 \le x_1 \le 1$, which is less than $\pi/2$, and on the initial geometry of the liquid free surface: $1{\cdot}21 < U_* < 1{\cdot}28$ for $7{\cdot}5\text{m} < R < 75$ m. This means that the total elastic energy U_* is dependent mainly on impact velocity the plate flexibility and only weakly on the initial shape of the liquid free surface. Inequality (54) can be improved by taking the energy of spray jets into account. This problem is not considered here.

9. Estimation of maximum bending stresses

In order to illustrate how to estimate the maximum amplitude of the bending stresses in the plate, the central-impact case is considered. The corresponding analysis for the edge impact is described in [24].

The parts $T_B(t)$, $P_B(t)$ and $T_{LE}(t)$ of the total elastic energy U_* during the penetration stage are depicted in Figure 14 as functions of time t. It is seen that the main contribution to the total energy U_* at the beginning of the penetration stage comes from the kinetic energy of the liquid flow T_{LE} and there is a time instant t_m, when the total energy is concentrated in the potential energy of the deformed plate

$$P_B(t_m) \approx U_*. \tag{55}$$

The maximum stress in the plate (thick line) and the stress at the plate midpoint (thin line) are shown in Figure 15. We may conclude that the stresses at the plate centre can be used to approximate the absolute maximum value of the bending stresses. It is important to notice that the bending stresses approach their maximum value at $t \approx t_m$ approximately.

Within the normal-mode approach the potential energy $P_B(t)$, $t > t_3$, is the sum of the mode contributions. Relative contributions of modal potential energies are depicted in Figure 16, where $P_1(t)$ is the potential energy of the first dry mode

$$P_1(t) = \beta \lambda_1^4 a_1^2(t) \tag{56}$$

and

$$\tilde{P}(t) = \beta \sum_{n=2}^{10} \lambda_n^4 a_n^2(t)$$

is the contribution to the total potential energy including the second to tenth mode. It is seen that the first mode gives the main contribution to the potential energy of the deformed plate. Therefore, we obtain from (55) and (56) that

$$a_1^2(t_m) \approx \frac{U_*}{\beta \lambda_1^4}. \tag{57}$$

Within the one-mode approximation, which may be used to describe the hydroelastic behavior of the plate during the penetration stage, system (25–26) gives (see [25])

$$(\alpha + S_{11})\ddot{a}_1 + \beta \lambda_1^4 a_1 = 0 \ (t > t_3), \tag{58}$$

where $\lambda_1 = \pi/2$, $S_{11} = (\pi/2)[J_0^2(\pi/2) + J_1^2(\pi/2)]$. The term f_1 in (25) is zero after the plate is totally wetted. The general solution of Equation (58) has the form

$$a_1(t) = C_1 \sin(\omega t + \delta), \tag{59}$$

where $\omega = \lambda_1^2 \sqrt{\beta/(\alpha + S_{11})}$, and both C_1 and δ have to be determined from initial conditions. We assume that the one-mode approximation correctly describes the evolution of the beam potential energy with time. If so, Equations (57) and (58) yield

$$C_1 = \sqrt{U_*/\beta}\lambda_1^{-2}, \ t_m = (\pi/2 - \delta)/\omega. \tag{60}$$

The quantity δ can be found by matching either the potential or the kinetic energy at the beginning of the penetration stage. For example, if $P(t_3)$ is specified, we obtain the following equation

$$\beta \lambda_1^4 C_1^2 \sin^2 \delta = P(t_3). \tag{61}$$

Dimensional bending stresses are given as

$$\sigma'(x', t') = -(E z_a / R) w_{xx}(Lx, (L^2/RV)t), \tag{62}$$

where z_a is the distance from the neutral axis in the beam cross-sectional area to the point where the stress is evaluated [2]. For a beam of constant thickness h, we have $z_a = h/2$ on the beam surface. Within the one-mode approximation the absolute maximum of the bending stresses $\sigma'_{\max}$ and the time t'_m can be found by using (60–62) as

$$\sigma'_{\max} \approx \sqrt{U_*} V z_a \sqrt{\frac{\rho L E}{J}}, \quad t'_m \approx \frac{2L^2}{\pi}\left(1 - \frac{2\delta}{\pi}\right)\sqrt{\frac{M_B + S_{11}\rho L}{EJ}}, \quad \delta = \arcsin\sqrt{P(t_3)/U_*}. \tag{63}$$

In the experimental conditions for the steel plate, formulae (63) provide $\sigma'_{\max} \approx 1867\mu$s and $t'_m \approx 0{\cdot}0075$s with $\delta = 0$, which reasonably correspond to the measured values $\sigma'_{\max} = 1600\mu$s and $t'_m = 0{\cdot}005$s. It should be noted that the connection between the elastic plate and the structure was more complicated in the experiment that in the simplified theoretical analysis here. By taking into account more realistic edge conditions, we may hope to reduce the differences between the estimated and the measured values.

The non-dimensional 'elastic' energy U_* in (63) has to be evaluated from the numerical solution of the original problem at the impact stage with all peculiarities of this stage taken into account. This fact reduces the practical importance of the approximate formula (63) for the value $\sigma'_{\max}$. On the other hand, we can use inequality (54) to estimate the stresses. The corresponding bound is depicted in Figure 17 by the broken line.

Let us denote the total length of the beam by L_B, then (54) and (63) lead to

$$\frac{|\sigma_{max}|}{\left(\frac{z_a}{L_B}\right) V \sqrt{\frac{J}{\rho E L_B^3}}} \leq \sqrt{\frac{\pi}{4}},$$

where $\sqrt{\pi/4} \approx 0{\cdot}88$. Experimental results for the same ratio and different impact velocities, plates and impact conditions [2] give the corresponding upper bound as 0·7. The obtained theoretical estimation overpredicts the experimental estimate but is simple and can be recommended for structural analysis of plates subject to wave-impact loads.

10. Conclusion

It has been demonstrated in the present paper that the normal-mode method is a powerful tool to treat the unsteady problem of elastic plate impact onto a liquid free surface which is slightly curved. The method was modified to avoid calculations of the hydrodynamic loads. The study focused on deflections of the plate and distribution of bending stresses. The original problem is reduced to a system of ordinary differential equations for the principal coordinates of the normal modes. The positions of the contact points are governed by nonlinear differential equations, which are incorporated into the system for the principal coordinates. It is important to notice that the numerical solution can be started from the initial instant of time, when the dimension of the wetted area of the plate is zero. The numerical algorithm does not require supercomputers and renders it possible to investigate details of the plate/liquid interaction.

The impact stage, during which the plate is wetted only partially, is divided into three phases. The peculiarities of the interaction are investigated for each phase. Impact conditions, for which Wagner's theory can be used, are distinguished. The phenomenon of the hydrodynamic load increase due to plate flexibility was revealed (blockage phenomenon). It is shown that a cavity attached to the plate may be formed just before the hydrodynamic loads become unbounded. The impact of an elastic plate with an attached cavity is analyzed.

Maximum bending stresses are obtained numerically and compared with the measured data. Calculated stresses overestimate the contributions of the higher modes. An explanation of the higher-mode generation is given. Higher modes are generated during the impact stage and are due to the effect of wetted-area expansion.

It is shown that the components of the energy of the plate/liquid system are strongly dependent on the impact conditions but the total energy is a rather stable quantity. The greater the kinetic energy of the spray jets is, the smaller the potential energy of the deformed plate will be. The obtained estimate of the potential energy leads to an estimate of the absolute maximum of the bending stresses, which corresponds reasonably well to the experimental

results. The obtained theoretical estimate can be used in the structural analysis of plates subject to wave impact.

Preliminary results of this work were reported at the International Workshops on Water Waves and Floating Bodies in 1997, 1998, 1999 and at the 7-th International Conference on Numerical Ship Hydrodynamics, 1999.

References

1. J.V. Aarsnes, *An Experimental Investigation of the Effect of Structural Elasticity on Slamming Loads and Structural Response*. *Technical Report*, MARINTEK A/S, Trondheim, Norway (1994).
2. O.M. Faltinsen, J. Kvålsvold and J.V., Aarsnes, Wave impact on a horizontal elastic plate. *J. Marine Sci. Technol.* (1997) 87–100.
3. J. Kvålsvold and O.M. Faltinsen, Hydroelastic modelling of slamming against the wetdeck of a catamaran. *Proc. Second Int. Conf. Fast Sea Transportation, FAST'93*, Yokohama, Japan (1993) pp. 681–697.
4. J. Kvålsvold and O.M. Faltinsen, Slamming loads on wetdeck of multihull vessels. In: O.M. Faltinsen, *et al*. (eds.), *Proc. Int. Conf. Hydroelasticity in Marine Technology*, Trondheim, Norway (1994) pp. 205–220.
5. J. Kvålsvold and O.M. Faltinsen, Hydroelastic modelling of wetdeck slamming on multihull vessels. *J. Ship Res.* 39 (1995) 225–239.
6. J. Kvålsvold, *Hydroelastic Modelling of Wetdeck Slamming on Multihull Vessels*. Doctoral/Thesis, Department of Marine Hydrodynamics, Norwegian Institute of Technology, MTA-report 100 (1994) 100 pp.
7. O.M. Faltinsen, The effect of hydroelasticity on ship slamming. *Phil. Trans. R. Soc. London* A355 (1997) 575–593.
8. S.L. Chuang, *Experimental Investigation of Dynamic Interaction Between Rectangular Elastic Plate and Fluid during Flat-Bottom Slamming*. Report 2411, Naval Ship Research and Development Center (1967) pp. 28.
9. L. Zhu and D. Faulkner, *Slamming Drop Tests for Small Scale SWATH Characteristic Model*. NAOE-94-34, Department of NAOE, University of Glasgow (1994) 63pp.
10. A.A. Korobkin, *Elastic Effects on Slamming*. NAOE-96-39, Department of NAOE, University of Glasgow (1996) 134pp.
11. A.A. Korobkin, Acoustic approximation in the slamming problem. *J. Fluid Mech.* 318 (1996) 165–188.
12. A.A. Korobkin, Wave impact on the center of an Euler beam. *J. Appl. Mech. Tech. Phys.* 39 (1998) 770–781.
13. A.A. Korobkin, Water impact problems in ship hydrodynamics. In: M. Ohkusu (ed.), *Advances in Marine Hydrodynamics*. Southampton: Computational Mech. Publ. (1996) 323–371.
14. A.A. Korobkin and T.I. Khabakhpasheva, Plane linear problem of the immersion of an elastic plate in an ideal incompressible fluid. *J. Appl. Mech. Tech. Phys.* 40 (1999) 491–500.
15. H. Wagner, Über Stoss- und Gleitvergänge an der Oberfläche von Flüssigkeiten. *Z. Angew. Math. Mech.* 12 (1932) S.193–235.
16. A.A. Korobkin and T.I. Khabakhpasheva, Plane problem on asymmetrical wave impact on an elastic plate. *J. Appl. Mech. Tech. Phys.* 39 (1998) 782–791.
17. A.A. Korobkin and V.V. Pukhnachov, Initial stage of water impact. *Ann. Rev. Fluid Mech.* 20 (1988) 159–185.
18. A.A. Korobkin, Initial asymptotics in the problem of blunt body entrance into liquid. Ph.D. Thesis. Novosibirsk: Lavrentyev Institute of Hydrodynamics (1985)
19. A.A. Korobkin, Wave impact on the bow end of a catamaran wet deck. *J. Ship Res.* 39 (1995) 321–327.
20. T.I. Khabakhpasheva and A.A. Korobkin, Wave impact on elastic plates. In: B. Mokin (ed.), *Proc. 12th Intern. Workshop on Water Waves and Floating Bodies*. Carry-le-Rouet, France (1997) pp. 135–138.
21. T.I. Khabakhpasheva and A.A. Korobkin, One-side inequalities in the problem of the wave impact. In: A.J. Hermans (eds.), *Proc. 13th Intern. Workshop on Water Waves and Floating Bodies*. Alphen aan den Rijn, Netherlands (1998) pp. 67–70.
22. I. Shibue, A. Ito and E. Nakayama, Structural response analysis of cylinders under water impact. In: O.M. Faltinsen, *et al*. (eds.), *Proc. Int. Conf. Hydroelasticity in Marine Technology*. Rotterdam: Balkema (1994) pp. 221–228.
23. A.A. Korobkin, Blunt-body penetration into a slightly compressible liquid. In: M. Tukin (eds.), *20th Symposium on Naval Hydrodynamics*. University of California, Santa Barbara, California (1994) pp. 179–186.
24. T.I. Khabakhpasheva and A.A. Korobkin, Energy conservation law in the problem of elastic plate impact onto liquid free surface. In: R.F. Beck and W.W. Schultz (eds.), *Proc. 14th Intern. Workshop on Water Waves and Floating Bodies*. Michigan (1999) pp. 72–75.
25. A.A. Korobkin and T.I. Khabakhpasheva, Periodic wave impact onto an elastic plate. *Preprint of the Proc. 7th Intern. Conference on Numerical Ship Hydrodynamics*. Nantes, France, 1999. pp. 7.3.1–7.3.19.